Depth-resolved magnetization reversal in nanoporous perpendicular anisotropy multilayers

B. J. Kirby,[1] M. T. Rahman,[2,3] R. K. Dumas,[4,5] J. E. Davies,[6] C. H. Lai,[2] and Kai Liu[4]
[1]*Center for Neutron Research, NIST, Gaithersburg, Maryland 20899, USA*
[2]*Materials Science and Engineering, National Tsing Hua University, Hsinchu 30043, Taiwan*
[3]*MINT Center, University of Minnesota, Minneapolis, Minnesota 55455, USA*
[4]*Physics Department, University of California, Davis, California 95616, USA*
[5]*Physics Department, University of Gothenburg, Gothenburg 41296, Sweden*
[6]*Advanced Technology Group, NVE Corporation, Eden Prarie, Minnesota 55344, USA*

(Received 25 September 2012; accepted 27 December 2012; published online 17 January 2013)

We have used polarized neutron reflectometry to study the field-dependent magnetizations of Co/Pt mulitlayers patterned via deposition onto nanoporous alumina hosts with varying pore aspect ratio. Despite the porosity and lack of long-range order, robust spin-dependent reflectivities are observed, allowing us to distinguish the magnetization of the surface multilayer from that of material in the pores. We find that as the pores become wider and shallower, the surface Co/Pt multilayers have progressively smaller high field magnetization and exhibit softer magnetic reversal—consistent with increased magnetic disorder and a reduction of the perpendicular anisotropy near the pore rims. These results reveal complexities of magnetic order in nanoporous heterostructures, and help pave the way for depth-resolved studies of complex magnetic heterostructures grown on prepatterned substrates. © *2013 American Institute of Physics*. [http://dx.doi.org/10.1063/1.4775819]

I. INTRODUCTION

Arrays of nanoscale magnetic elements not only have important applications in ultrahigh density bit patterned recording media[1,2] and spintronic devices[3] but also facilitate fundamental studies of spatially confined magnetism.[4–6] Deposition of magnetic films[7,8] and multilayers[9,10] onto nanoporous host matrices has been shown as a simple and cost-effective method for achieving such arrays over macroscopic areas. When a thin layer is deposited, most of the materials are on top of the growth matrix, replicating the nanoporous structure. The lateral confinement within the film plane provides a means to tailor the magnetization reversal mechanisms, leading to attractive networked media[11] with enhanced coercivity and improved thermal stability.[7,8] As the deposition continues, more and more material enters into the pores of the template. The amount of material deposited on the porous surface as compared to the amount that settles inside the pores or along the pore edges depends critically on the pore aspect ratio $A = h/D$, where D is the pore diameter, and h is the pore depth. Magnetometry and first order reversal curve (FORC) measurements of nanoporous Co/Pt have shown that the pore aspect ratio has a profound effect on the magnetization reversal of the sample as a whole, both by changing the size of the lateral dimension with respect to the domain wall size, and by changing the amount of magnetic material that can enter the pore.[9] These measurements indicate that for high aspect ratio, when the Co/Pt is largely confined to the sample surface, the pores act as pinning sites, and magnetization reversal is dominated by motion of highly pinned domain walls. Conversely, when the aspect ratio is decreased and more Co/Pt is deposited in the pores, the magnetic reversal appears more consistent with rotation. However, distinguishing the magnetization of the surface multilayer from underlying magnetic material in the pores can be exceedingly difficult with magnetometry alone, which measures the collective magnetic response and lacks any spatial sensitivity. This challenge in probing depth-dependent magnetization reversal is common in a wide variety of magnetic nanostructures prepared on pre-patterned substrates, such as bit patterned media grown on patterned pillars[2] and tilted media deposited on self-assembled nanospheres.[12] Polarized neutron reflectometry (PNR) is a technique that can provide such a depth sensitivity. But as it is sensitive to the in-plane average of the depth profile, it is most commonly used to study films or multilayers that are either compositionally continuous in the plane, or are patterned to exhibit long-range in-plane order. In this work, we report a PNR study of nanoporous Co/Pt multilayer samples, heterogeneous both laterally in the film plane and vertically along the film depth, and how pore aspect ratio affects the field-and depth-dependent magnetization.

II. SAMPLE FABRICATION

Three nanoporous anodized aluminum oxide (AAO) matrices with hexagonal close-packed (hcp) pores of varying A were produced by anodic oxidation of 50 nm Al films on Ti-capped Si substrates in sulfuric acid held at a 25 V potential followed by etching in 5% phosphoric acid. The pore diameter, spacing, and depth are all tuned by varying the etch time. Multilayers of 8 nm Pt seed/[0.5 nm Co/2 nm Pt]$_5$ were deposited onto the porous matrices via dc magnetron sputtering, resulting in magnetic multilayer samples with differing patterning dimensions. Details of the sample preparation procedures have been reported earlier.[9] Top-view scanning electron microscopy (SEM) and cross-sectional transmission electron microscopy (TEM) images indicate aspect ratios of $A = 3.2$ ($D = 13$ nm, $h = 41$ nm), $A = 1.6$ ($D = 20$ nm, $h = 31$ nm), and $A = 0.7$ ($D = 28$ nm, $h = 20$ nm) for the samples. Figure 1 shows a

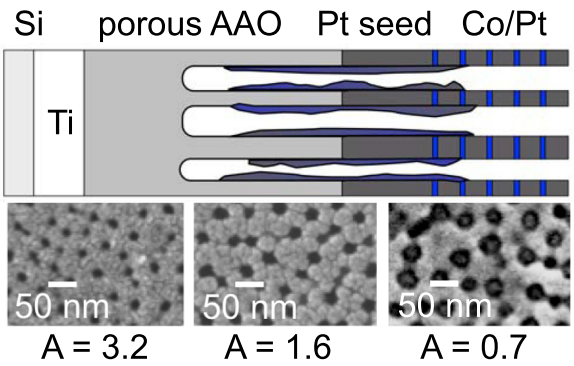

FIG. 1. Schematic of the cross-sectional sample structure (top), and top-view SEM images of the sample surfaces (bottom).

cartoon representation of the sample structure, as well as SEM images of the three sample surfaces. As A decreases, the pore size increases and the depth decreases. For samples with $A = 3.2$ and 1.6, the deposited Co/Pt multilayers are primarily on top of the AAO, which we will refer to as the "surface layer," and around the perimeter of the pores. However, for $A = 0.7$, a significant portion of Co/Pt is deposited inside the pores in addition to the surface layer.

III. EXPERIMENT

Magnetic properties have been measured by vibrating sample magnetometry (VSM). Major hysteresis loops of the samples are shown in Fig. 2, both with field perpendicular to (dashed lines) and in the plane of the sample (solid lines). All three samples exhibit a pronounced perpendicular magnetic anisotropy with an enhanced coercivity of around 0.15 T in the out-of-plane geometry, an order of magnitude larger than in continuous Co/Pt films.[9] This is due to the confined sample lateral dimensions which impedes the nucleation and motion of domain walls and forces more of the moments to reverse via rotation. There are only subtle variations as A is decreased, e.g., a gradual reduction of the out-of-plane loop squareness. The loops do not exhibit distinct

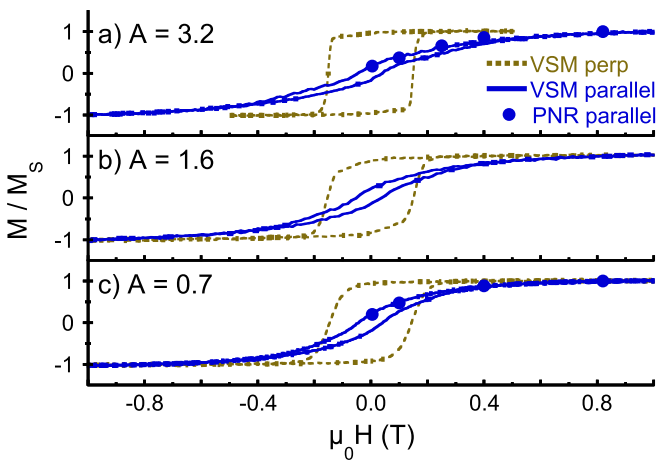

FIG. 2. Field-dependent magnetization normalized by the saturation magnetization (M_S) for the three samples as measured with VSM, with field applied perpendicular (dashed lines), and parallel (solid lines) to the sample surface. Solid symbols correspond to the integrated in-plane magnetization profiles as measured with PNR.

steps that could be used to clearly distinguish the magnetization of the surface multilayers on top of AAO from the magnetization of materials in the pores.

Specular PNR is sensitive to the nuclear and magnetic depth profiles of films and multilayers, probing along the surface normal (z) direction while averaging over planar features.[13,14] Specular reflection occurs at the interfaces of regions with differing indices of refraction (a function of nuclear composition and magnetization), and as such, sharp interfaces yield reflectivity features that are, in general, easier to detect and interpret. Evident from Fig. 1 SEM images, the porous samples discussed here clearly deviate from this PNR ideal, and while there is a significant body of work showing the utility of PNR for characterization of patterned surfaces,[15–17] such work has primarily focused on off-specular diffraction from large (μm scale) elements that exhibit long-range order. While less common, PNR has also been used to study films comprised of magnetic elements lacking long-range order, such as Fe islands,[18] CoFe nanoparticles embedded in Al_2O_3,[19] and Fe oxide nanoparticles.[20] If the in-plane elements are too small to be distinguished by the neutron beam, the layers can be treated as uniform mixtures, for example, as has been done with unpolarized neutron reflectometry measurements of block copolymer films.[21] Such is the case for the measurements described here, as the neutron coherence length is approximately 10–100 μm, several orders of magnitude larger than the pore diameters. Thus, each neutron interacts with both porous and contiguous regions, and the specular scattering is representative of the average in-plane composition as a function of depth.

PNR measurements on samples with surface area ranging from approximately $15 - 50\,\mathrm{mm}^2$ were conducted on the NG-1 reflectometer at the NIST Center for Neutron Research. A monochromatic beam was polarized spin-up (+) or spin-down (−) with respect to the sample field, and the scattered beam was spin-analyzed and measured as a function of scattering vector along the sample surface normal, Q_z. As no significant spin-flip scattering was observed for any measurement, only the non spin-flip reflectivities R^{++} and R^{--} are discussed in this work. The data were corrected for background, beam polarization, and beam footprint. Rocking curves about the specular reflection revealed no evidence of significant off-specular scattering, as expected given the small pore size. For specular PNR, the component of the magnetization perpendicular to the sample surface is not detectable, so measurements were conducted in a decreasing in-plane field after saturating along the perpendicular direction, and then applying a near-saturating 0.82 T in-plane field. The $A = 3.2$ and $A = 0.7$ samples were measured as a function of decreasing field, while only the near-saturation state was measured for the $A = 1.6$ sample.

Figure 3 shows the fitted PNR data measured at 0.82 T, plotted as Fresnel-normalized reflectivity (the specular reflectivity of the sample divided by the theoretical reflectivity of the bare Si substrate) in order to visualize features across a wide Q_z-range. For clarity, Fig. 3 shows only the low-Q_z regions where spin-splitting is most apparent; however, we note that oscillations were measured and well fitted out to $Q_z \approx 0.6\,\mathrm{nm}^{-1}$. The pronounced oscillations in Fig. 3

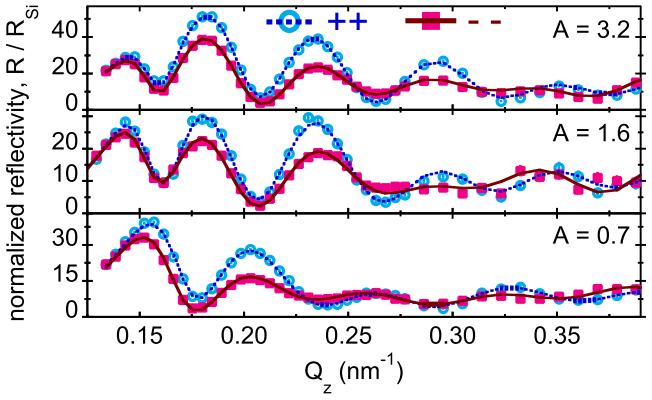

FIG. 3. Measured PNR spectra (symbols) at 0.82 T for the $A = 3.2$ (top), $A = 1.6$ (middle), and $A = 0.7$ (bottom) samples. Solid and dashed lines are fits to the data. Note the different vertical scales for the three panels. Error bars correspond to ± 1-σ, and are smaller than the point size for much of the data shown.

indicate the interfaces are discrete enough to be distinguished, while sample-dependent differences demonstrate the sensitivity to variations in pore size. Data measured at lower fields (not shown) are similar to that in Fig. 3, showing only a reduced spin-splitting, as expected. Reflectivities R^{++} and R^{--} are functions of the spin-dependent scattering length density depth profiles,[13,14]

$$\rho^{++}(z) = \rho_N + CM, \tag{1}$$

$$\rho^{--}(z) = \rho_N - CM, \tag{2}$$

where ρ_N is indicative of the nuclear composition, M is the in-plane projection of the sample magnetization parallel to the applied field, and C is a constant.[22] Therefore, the sample magnetization is manifest as a splitting between R^{++} and R^{--}. Fig. 3 reveals significant splitting for all three samples, indicating sensitivity to the magnetic depth profiles.

IV. ANALYSIS

Model-fitting of the PNR data was carried out using the REFL1D software package,[23] yielding the nuclear and magnetic depth profiles shown in Figure 4. Layers of native SiO_2, Ti, and non-porous "bulk" AAO are treated as non-magnetic slabs, joined by Gaussian transition functions. The thickness, ρ_N, and transition widths for the Ti and bulk AAO layers were free parameters for fitting. To account for pores partially filled with Co/Pt, porous AAO regions are modeled in a "free-form" fashion, with four control points of variable ρ_N and M, connected by spline functions. The models for each sample were constrained to have field-independent nuclear profiles, with only the magnetization of the four control points allowed to vary. Since the Q_z range being probed is well below, where we would be sensitive to the individual Co and Pt layers in the multilayer stacks, and since the multilayer structure is unlikely to be in uniform registry across the width of the sample, the surface layer of porous $[Co/Pt]_5$ on top of AAO is treated as a single magnetic layer[24,25] with a rough air interface (rms roughness equal to three times the layer thickness). The magnetization profiles can be compared

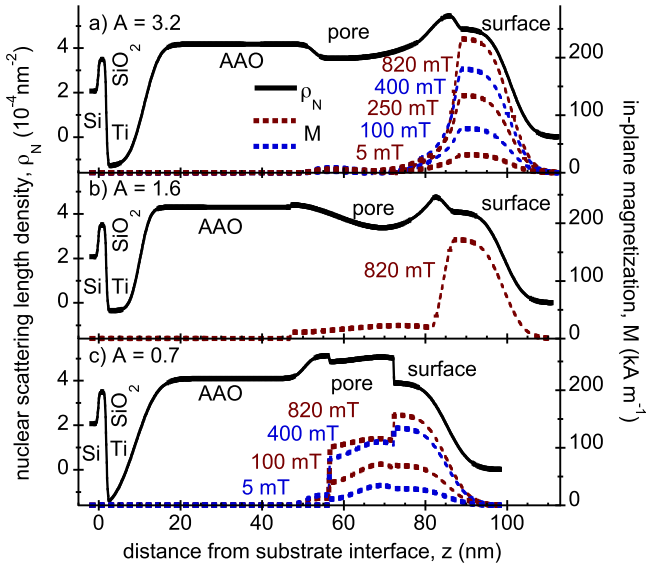

FIG. 4. Nuclear (solid, left axis) and magnetic (dashed, right axis) depth profiles for the (a) $A = 3.2$, (b) $A = 1.6$, and (c) $A = 0.7$ samples.

with VSM results by integrating the profiles over all z. These integrals normalized by the values at 0.82 T are shown as solid symbols in Fig. 1. This comparison reveals excellent agreement between the two techniques, providing a strong confirmation of the model fitting. To facilitate interpretation, Figure 5 shows the portions of the 0.82 T profiles corresponding to the porous surface regions, directly below scaled cross-sectional TEM images.

Vertical bars overlaid on the plot delineate the surface Co/Pt multilayer (right side of the bar) from the rest of the sample (left side). Comparison with the TEM images illustrates a direct correspondence between key distinguishing features in the neutron profiles and distinct regions of the porous surfaces. First, consider the $A = 3.2$ sample, which has deep, narrow pores. The region $88\,\text{nm} < z < 100\,\text{nm}$ corresponds to an average of Co/Pt multilayer and empty pores. Pt has a significantly larger ρ_N $(6.3 \times 10^{-4}\,\text{nm}^{-2})$ than Co $(2.2 \times 10^{-4}\,\text{nm}^{-2})$,[26] and is non-magnetic. Thus, the Pt seed layer is evident in the profiles as a spike in ρ_N

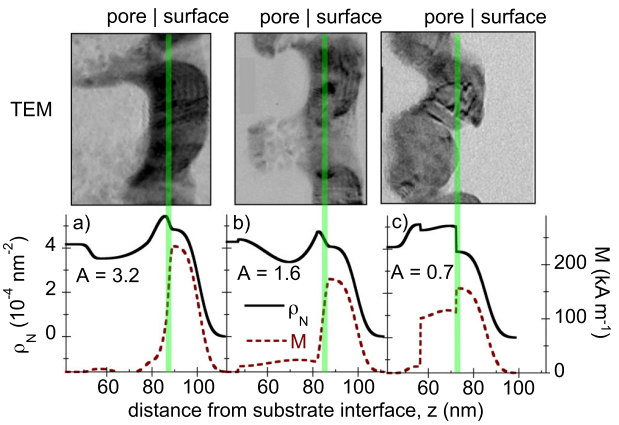

FIG. 5. Nuclear (solid, left axis) and magnetic (dashed, right axis) depth profiles, and corresponding cross-sectional TEM images for (a) $A = 3.2$, (b) $A = 1.6$, and (c) $A = 0.7$ samples. The scale of the TEM images matches that of the depth PNR profiles. For each sample, the surface Co/Pt multilayer is delineated by a vertical bar.

and a sharp dip in M between $80\,\text{nm} < z < 88\,\text{nm}$. From $50\,\text{nm} < z < 80\,\text{nm}$, ρ_N gradually decreases with decreasing z, while M drops effectively to zero. This region corresponds to AAO, empty pores, and residual Co and Pt that has been deposited along the pore walls. For the $A = 1.6$ sample, the pores are wider and shallower. The surface profile is similar to that of the $A = 3.2$ sample, but with reduced ρ_N, due to the increased pore diameter. The $A = 0.7$ sample is significantly different than the other two, as the pores are shallow and wide enough to have Co/Pt multilayers deposited to the bottom, not just onto the walls. The surface Co/Pt multilayer on top of AAO is again clearly distinguishable, with a further decrease in ρ_N due to increased pore diameter. However, in this case, the Pt seed layer portion of the surface network is not directly distinguishable, as it significantly overlaps with the Co/Pt multilayer deposited inside the pores. Thus, the nuclear profiles show excellent agreement with the TEM images, while simultaneously providing context for the magnetic profiles.

For each of the samples, the surface profiles correspond to an average of only two components—Co/Pt multilayer with an expected nuclear scattering length density $\rho_{\text{CoPt}} = 5.5 \times 10^{-4}\text{nm}^{-2}$ (for 20% Co and 80% Pt),[26] and empty pores with $\rho_N = 0$. Thus, the sample surface can be analyzed as a layer of dilute CoPt with ρ_N that falls off with increasing z due to the large average roughness of the porous structure. The volume fraction of the surface occupied by the Co/Pt network is

$$v_f = \frac{\rho_N}{\rho_{CoPt}}. \tag{3}$$

Additionally, the nuclear scattering length density can be used to infer the relative circumference of the pores η. Assuming a hcp arrangement of identical circles, the maximum volume fraction that can be occupied by pores is $v_{hcp} = \frac{\pi\sqrt{3}}{6}$, and the ratio of the pore circumference l_{pore} to the maximum possible pore circumference l_{max} can be expressed as

$$\eta = \frac{l_{pore}}{l_{max}} = \sqrt{\frac{1 - v_f}{v_{hcp}}}. \tag{4}$$

This quantity can be thought of as a measure of the amount of "pore rim" in the porous surface region. Accounting for the empty pores, the magnetization of the Co/Pt multilayers on top of the contiguous AAO is

$$M_{CoPt} = \frac{M}{v_f}. \tag{5}$$

Figure 6 shows the A-dependencies of v_f (a), η (b), and the near-saturation surface magnetization both in absolute units (c) and after normalization (d). The values are determined from the PNR model fitting, and are shown with 2-σ uncertainty calculated using a Markov chain Monte Carlo algorithm.[23,27,28] As A increases, the volume fraction occupied by Co/Pt increases, while the fraction occupied by pore rim decreases. The determined values of v_f are within 10% of what would be expected based on hcp arrangements of

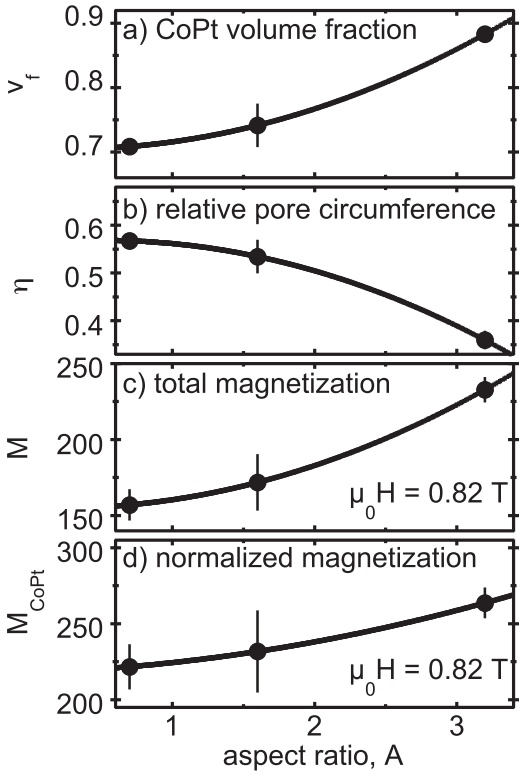

FIG. 6. Aspect ratio dependencies of (a) CoPt surface coverage, (b) relative pore circumference, (c) total surface near-saturation magnetization, and (d) normalized surface near-saturation magnetization. Solid lines are guides to the eye. Error bars correspond to ± 2-σ.

pores with the diameters estimated from SEM—another strong confirmation of the model fitting. Since v_f increases with A, it is not surprising that the near-saturation surface magnetization M does the same. However, it is notable that this trend remains even after correcting for pore size, as the near-saturation M_{CoPt} also increases progressively with increasing A. Figure 7(a) shows the field dependence of M_{CoPt} for the $A = 3.2$ and the $A = 0.7$ samples.

While the surface Co/Pt multilayer of the $A = 3.2$ sample has a significantly higher near-saturation magnetization than does the $A = 0.7$ sample, the latter is magnetically softer in-plane, as the low field values are similar for both samples. Both of these effects are evidence of "rounding" of the Co/Pt multilayer near the rims of the pores, as is clearly seen in the Fig. 5 TEM images. The near-rim regions are likely to be highly disordered, resulting in locally reduced magnetization and perpendicular anisotropy. As A is decreased, the pore circumference increases, and such near-rim regions constitute a progressively a larger fraction of the total surface Co/Pt multilayer, resulting in a net reduction in near-saturation magnetization, and in effective anisotropy. This is consistent with the gradual reduction of the squareness of the out-of-plane hysteresis loops as A is reduced (Fig. 2).

For the $A = 0.7$ sample, we can also compare the field-dependent magnetization of the surface to the average field-dependent magnetization of the filled pores. As the nuclear profile for the sub-surface region corresponds to more than just Co/Pt and empty space (averaging with Pt seed layer, AAO, depth-dependent amount of sidewall material, etc.), it is much more challenging to extract a normalized Co/Pt magnetization.

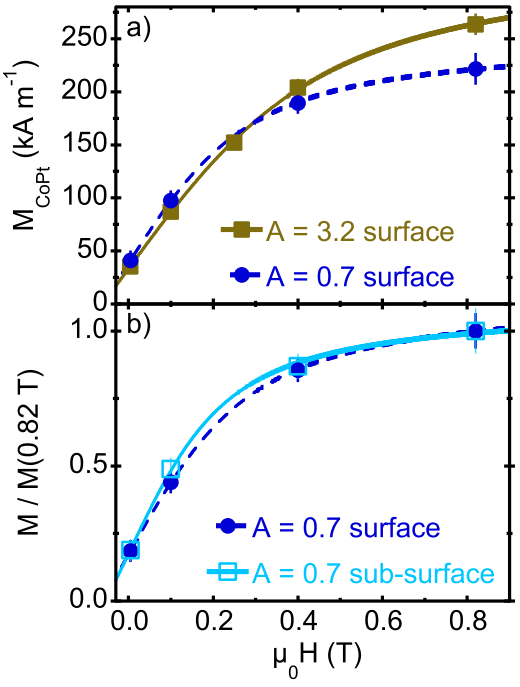

FIG. 7. (a) Field-dependence of the normalized surface Co/Pt magnetization as determined from PNR (open symbols). (b) Comparison of surface and sub-surface Co/Pt magnetizations for the $A = 0.7$ sample. Error bars correspond to ± 2-σ. Lines are guides to the eye.

Thus, in Fig. 7(b) we compare the surface and the average sub-surface magnetizations, normalized by the respective high-field values. We observe that the magnetizations of the surface and the sub-surface respond to field essentially identically. Previous FORC measurements of this sample[9] suggest that the surface and sub-surface magnetizations are largely decoupled. Therefore, we conclude that the similar magnetization reversal behaviors are due to the comparable restricted lateral dimensions of the Co/Pt on the AAO surface and in the pores. Both the pore diameter and the pore edge-to-edge distance are similar to the typical domain size of Co/Pt multilayers ($\sim$15 nm),[29] allowing for magnetization reversal to proceed through rotation in both the surface and sub-surface regions.

V. CONCLUSION

We have used PNR to resolve the nuclear and magnetic depth profiles of a series of Co/Pt multilayers deposited onto nanoporous AAO templates with varying aspect ratio. The nuclear profiles are consistent with cross-sectional TEM images, and the field dependencies of the integrated magnetic profiles show excellent agreement with VSM measurements. From the profiles, the field-dependent magnetization of the surface Co/Pt can be distinguished from that of material in the pores. We observe that as the pores become wider and shallower, the surface Co/Pt exhibits a reduction in saturation magnetization and a softer magnetization reversal, attributable to significant magnetic disorder near the rims of the pores. This work reveals complexities of magnetic order in nanoporous heterostructures, and the utility of PNR for investigation of depth-dependent magnetic properties in such materials.

ACKNOWLEDGMENTS

Support from the NSF Materials World Network program (DMR-1008791) is gratefully acknowledged. We thank B. B. Maranville, J. A. Borchers, and P. A. Kienzle of NIST for valuable discussions.

[1]S. H. Sun, C. B. Murray, D. Weller, L. Folks, and A. Moser, Science **287**, 1989 (2000).
[2]O. Hellwig, A. Moser, E. Dobisz, Z. Z. Bandic, H. Yang, D. S. Kercher, J. D. Risner-Jamtgaard, D. Yaney, and E. E. Fullerton, Appl. Phys. Lett. **93**, 192501 (2008).
[3]S. Mangin, D. Ravelosona, J. A. Katine, M. J. Carey, B. D. Terris, and E. E. Fullerton, Nature Mater. **5**, 210 (2006).
[4]S. D. Bader, Rev. Mod. Phys. **78**, 1 (2006).
[5]L. J. Heyderman, F. Nolting, D. Backes, S. Czekaj, L. Lopez-Diaz, M. Klaui, U. Rudiger, C. A. F. Vaz, J. A. C. Bland, R. J. Matelon, U. G. Volkmann, and P. Fischer, Phys. Rev. B **73**, 214429 (2006).
[6]K. Liu, S. M. Baker, M. Tuominen, T. P. Russell, and I. K. Schuller, Phys. Rev. B **63**, 060403 (2001).
[7]J. A. Barnard, H. Fujiwara, V. R. Inturi, J. D. Jarratt, T. W. Scharf, and J. L. Weston, Appl. Phys. Lett. **69**, 2758 (1996).
[8]K. Liu and C. L. Chien, IEEE Trans. Magn. **34**, 1021 (1998).
[9]M. T. Rahman, R. K. Dumas, N. N. Shams, Y.-C. Wu, K. Liu, and C. H. Lai, Appl. Phys. Lett. **94**, 042507 (2009).
[10]M. T. Rahman, N. N. Shams, C. H. Lai, J. Fidler, and D. Suess, Phys. Rev. B. **81**, 014418 (2010).
[11]J. G. Zhu and H. Fang, IEEE Trans. Magn. **34**, 1609 (1998).
[12]M. Albrecht, G. Hu, I. L. Guhr, T. C. Ulbrich, J. Boneberg, P. Leiderer, and G. Schatz, Nat. Mater. **4**, 203 (2005).
[13]C. F. Majkrzak, Physica B **221B**, 342 (1996).
[14]C. F. Majkrzak, K. V. O'Donovan, and N. F. Berk, in *Neutron Scattering From Magnetic Materials*, edited by T. Chatterji (Elsevier Science, New York, 2005).
[15]H. Fritzsche, M. J. V. Bael, and K. Temst, Langmuir **19**, 7789 (2003).
[16]S. Langridge, L. A. Michez, M. Ali, C. H. Marrows, B. J. Hickey, T. R. Charlton, R. M. Dalgliesh, M. Toohey, E. W. Hill, S. McFadzean, and J. N. Chapman, Phys. Rev. B **74**, 014417 (2006).
[17]K. L. Krycka, B. B. Maranville, J. A. Borchers, F. J. Castano, B. G. Ng, J. C. Perkinson, and C. A. Ross, J. Appl. Phys. **105**, 07C120 (2009).
[18]V. V. Krishnamurthy, S. G. E. te Velthuis, S. Srinath, P. Mani, and G. J. Mankey, J. Magn. Magn. Mater. **286**, 432 (2005).
[19]S. Bedanta, O. Petracic, X. Chen, J. Rhensius, S. Bedanta, E. Kentzinger, U. Rucker, T. Bruckel, A. Doran, A. Scholl, S. Cardoso, P. P. Freitas, and W. Kleeemann, J. Phys. D: Appl. Phys. **43**, 474002 (2010).
[20]D. Mishra, M. J. Benitez, O. Petracic, G. A. B. Confalonieri, P. Szary, F. Brussing, K. Theis-Brohl, A. Devishvili, A. Vorobiev, O. Konovalov, M. Paulus, C. Sternemann, B. P. Toperverg, and H. Zabel, Nanotechnology **23**, 055707 (2012).
[21]X. Zhang, B. C. Berry, K. G. Yager, S. Kim, R. L. Jones, S. Satija, D. L. Pickel, J. F. Douglas, and A. Karim, ACS Nano **11**, 2331 (2008).
[22]$C = 2.853 \times 10^{-7}$, for M in kA m^{-1} and ρ in nm^{-2}.
[23]B. J. Kirby, P. A. Kienzle, B. B. Maranville, N. F. Berk, J. Krycka, F. Heinrich, and C. F. Majkrzak, Curr. Opin. Colloid Interface Sci. **17**, 44 (2012).
[24]B. J. Kirby, S. M. Watson, J. E. Davies, G. T. Zimanyi, K. Liu, R. D. Shull, and J. A. Borchers, J. Appl. Phys. **105**, 07C929 (2009).
[25]B. J. Kirby, J. E. Davies, K. Liu, S. M. Watson, G. T. Zimany, R. D. Shull, P. A. Kienzle, and J. A. Borchers, Phys. Rev. B **81**, 100405 (2010).
[26]M. R. Fitzsimmons and C. F. Majkrzak, in *Modern Techniques for Characterizing Magnetic Materials*, edited by Z. Zhu (Kluwer, New York, 2005).
[27]BIPM, IEC, IFCC, *et al.*, Evaluation of measurement data - Supplement 1 to the "Guide to the expression of uncertainty in measurement": Propagation of distributions using a Monte Carlo method in Joint Committee for Guides in Metrology, 101 JCGM Joint Committee for Guides in Metrology (2008).
[28]J. A. Vrugt, C. J. F. T. Braak, C. G. H. Diks, D. Higdon, B. A. Robinson, and J. M. Hyman, Int. J. Nonlinear Sci. Numer. Simul. **10**, 273 (2009).
[29]R. Ploessl, J. N. Chapman, M. R. Scheinfein, J. L. Blue, M. Mansuripur, and H. Hoffmann, J. Appl. Phys. **74**, 7431 (1993).